The Fredrickson-Andersen model with random pinning on Bethe lattices and its MCT transitions

Harukuni Ikeda[1] , Kunimasa Miyazaki[1] and Giulio Biroli[2,3]

[1] *Department of Physics, Nagoya University - Nagoya 464-8602, Japan*
[2] *IPhT, CEA/DSM-CNRS/URA 2306, CEA Saclay, F-91191 Gif-sur-Yvette Cedex, France.*
[3] *Laboratoire de Physique Statistique, Ecole Normale Supérieure, PSL Research University, 24 rue Lhomond, 75005 Paris, France.*

arXiv:1609.02683v1 [cond-mat.dis-nn] 9 Sep 2016

PACS 64.70.Q- – Theory and modeling of the glass transition
PACS 05.20.-y – Classical statistical mechanics
PACS 05.50.+q – Lattice theory and statistics (Ising, Potts, etc.)

Abstract – We investigate the dynamics of the randomly pinned Fredrickson-Andersen model on the Bethe lattice. We find a line of random pinning dynamical transitions whose dynamical critical properties are in the same universality class of the A_2 and A_3 transitions of Mode Coupling Theory. The A_3 behavior appears at the terminal point, where the relaxation becomes logarithmic and the relaxation time diverges exponentially. We explain the critical behavior in terms of self-induced disorder and avalanches, strengthening the relationship discussed in recent works between glassy dynamics and Random Field Ising Model.

Introduction. – It still remains a major challenge to fully understand the origin of the dramatic slowing down of the dynamics of supercooled liquids near the glass transition point with little, if any, sign of structural orders. Many supercooled liquids display rich and universal dynamical behavior such as the two-step and non-exponential relaxation of the correlation functions, the super-Arrhenius dependence of the relaxation time, and spatially heterogeneous dynamics [1–3].

There are many theories attempting to describe the glass transition [2,3]. The mode coupling theory (MCT) is very successful in describing semi-quantitatively the time dependence of the density correlation functions of the supercooled liquids at relatively high temperatures [2, 4, 5]. However, it is known that MCT fails to describe the dynamics at low temperatures. MCT predicts an artificial divergence of the relaxation time well above the experimental glass transition temperature [2, 6].

It is now considered that MCT is part of the random first order transition (RFOT) theory, which is a thermodynamic theoretical approach for the glass transition inspired by the similarity between supercooled liquids and some mean-field spin glass models [7]. MCT has the same mathematical structure as that of the p-spin spherical model (PSM) which is a mean-field model of the RFOT [7–9]. Curiously, a different theory also predicts MCT-like dynamics at the mean-field level. The dynamical facilitation scenario (DF) claims that the glass transition is a purely dynamical transition *without* any thermodynamic singularity [3, 10]. DF is based on the kinetically constrained models (KCM), which have trivial thermodynamic properties but show complex glassy slow dynamics [10, 11]. The Fredrickson-Andersen model (FA), as well as other KCMs, has been shown to display the same scaling law of that of MCT in the mean-field limit [12–14].

The fact that completely different theories (one is thermodynamic and the other is kinetic) predict similar dynamics—and similar to MCT—in the mean-field limit suggests that there is an underlying universality hidden in MCT. This was indeed already discussed in [15], where the MCT scaling laws were obtained by a Landau-like expansion. Recently, it was shown that the MCT criticality is related to the one of the Random Field Ising Model (RFIM) [16, 17] and Franz and Sellitto have shown that the finite size scaling of the critical dynamics of the FA model on the Bethe lattice are indeed consistent with that of the RFIM [18].

In this work, we investigate thoroughly the universal structure of MCT by focusing on more general cases (always in the KCM context), studying whether the relationship with MCT still holds, and unveiling its physical content. In order to do so, we take advantage of recent

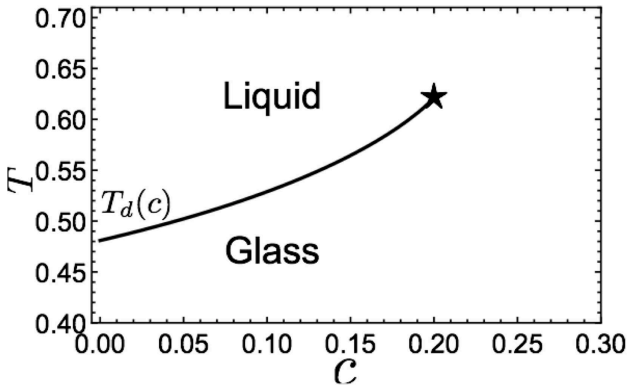

Fig. 1: The phase diagram of the model. The solid line denotes the putative A_2 transition line, $T_d(c)$. The filled star denotes the putative A_3 transition point, $c_c = 0.2$ and $T_c = T_d(c_c) \approx 0.621$.

results on the glass transition of randomly pinned systems [19–26], a fluid where a fraction of constituent particles are frozen or pinned. Theoretical analysis [23,27] predicts that by pinning a fraction c of particles from an equilibrium configuration at temperature T, the glass transition temperature $T(c)$ rises until it reaches a terminal critical point where it ends. The properties of the glass transition remain the same along the line but change at the terminal point. MCT predicts several anomalous dynamical behaviors for randomly pinned systems [20, 28, 29]. It predicts an MCT critical line where the transition remains, in the MCT terminology, of A_2 type, until the terminal point is reached where it becomes A_3 type. The dynamical behavior at the A_3 transition is qualitatively different. For example, the correlation function exhibits single logarithmic decay [30], instead of the usual two-step relaxation [5]. The relaxation time increases exponentially toward the A_3 transition point, while it increases algebraically toward the A_2 transition point [30]. Moreover, the critical behavior at the terminal point was shown to be related to the critical behavior of the RFIM at its continuous transition along the hysteresis line [17, 27, 28, 31] and not at its spinodal transition. The randomly pinned FA model thus provides a very useful setting to analyze the universal structure of MCT. Our aim will be on the one hand to check that the properties of the dynamical transition do not vary along the critical line induced by pinning and coincide with the ones predicted by MCT for the A_2 singularity and on the other hand that they do change at the terminal point, where instead they becomes the one predicted by MCT for the A_3 singularity. We shall also analyze the relationship with the RFIM and work out the physical mechanism behind it. In the a previous study, two of us have already investigated the static properties of the FA model with random pinning and indeed found some evidences of the scenario presented above [26].

Model and phase diagram. – We consider the FA model with random pinning on the regular random graph with connectivity $z = k + 1 = 4$ [26]. The Hamiltonian of the model is given by $H = -\frac{1}{2}\sum_{i=1}^{N}\sigma_i$, where $\sigma_i \in \{-1, +1\}$ denotes the binary spin variable on the i-th site. We pick up a fraction (denoted as c) of spins randomly from N spins and "pin" them. The pinned spins are not allowed to move from their initial equilibrium configuration. The time evolution rule of the model is the following [13]. We randomly select a spin and flip it with the probability $w(\sigma_i \to -\sigma_i) = \min\{1, e^{-\sigma_i/T}\}$ if the spin is *not* pinned and there are more than $f = 2$ number of downward spins in its neighbor. Otherwise, we do not flip the spin [26]. We use N iterations of this process as a unit of time. To characterize the slow dynamics, we observe the persistence function, $\phi(t)$, which is the fraction of the unflipped spins in the time span $[0, t]$. The analysis of the long time limit of the persistence function, $\phi = \lim_{t\to\infty}\phi(t)$, is particularly simple [13], since it can be mapped into the bootstrap percolation (BP) problem [32]. In the previous paper, we have calculated ϕ analytically as a function of T and c [26]. The phase diagram from ϕ is shown in Fig. 1. The solid line, $T_d(c)$, is the transition line. When $T > T_d(c)$, the system is in the "liquid phase" characterized by the low ϕ value and when $T > T_d(c)$, the system is in the "glass phase" characterized by the high ϕ value. $T_d(c)$ rises with increasing c and terminates at $(c_c, T_c) \approx (0.2, 0.621)$. Approaching $T_d(c)$ for $c < c_c$, ϕ changes discontinuously [26] as it would happen at an A_2 transition in the MCT terminology. Just below $T_d(c)$, ϕ changes as $\phi - \phi_d(c) \propto (T - T_d(c))^{1/2}$, where $\phi_d(c)$ is the fraction of the frozen spin at the transition temperature. On the other hand, at (c_c, T_c), ϕ behaves differently as $\phi - \phi_d(c_c) \propto (T - T_c)^{1/3}$, where ϕ changes continuously but singulary as MCT predicts for the A_3 transition [26]. Note that ϕ only contains information about the long time limit. It is still unclear how the above singularities of ϕ affect the explicit time dependent dynamical quantities of the system, especially how the dynamics is altered at the terminal point. Below, we show that those dynamical quantities indeed show the singular behaviors characteristic of A_2 and A_3 transitions.

Persistence Function and Critical Dynamic Scaling. – Hereafter, we investigate the dynamical properties of this model in more detail. We perform the Monte Carlo simulation (MC) by the faster-than-clock algorithm [33]. The systems size is $N = 2^{18}$ unless specifically mentioned, which is large enough to neglect the finite size effects. In this section, we focus on the time dependence of the persistence function, $\phi(t)$, and vary the temperature at fixed c. First, we present the results far from the terminal point. In this case, the dynamics should be of the standard A_2 type. This is indeed the case, as we show in Fig. 2 for $c = 0.05$ and $c = 0.1$. The transition temperatures are $T_d(c = 0.05) \approx 0.502$ and $T_d(c = 0.1) \approx 0.529$, respectively. As we approach $T_d(c)$ from above, the relaxation

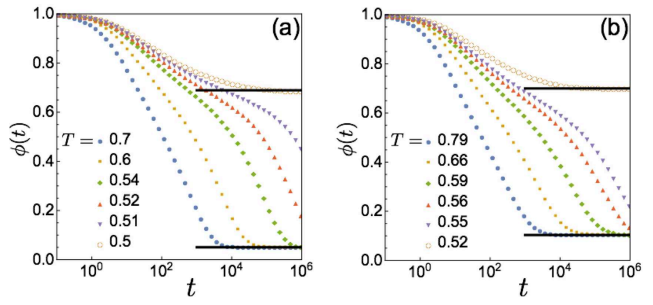

Fig. 2: Persistence functions approaching the random pinning transition (not at the terminal point). (a) The results for $c = 0.05$. The filled symbols denote the results of numerical simulation where the average is taken over 10 independent samples. The solid lines denote the fraction of the frozen spins estimated by the analytical equation. $\phi(t)$ converges to the value the fraction of the frozen spins in the long time limit. (b) The same data for $c = 0.1$.

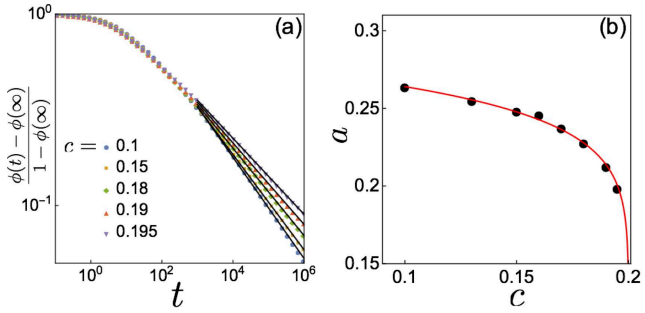

Fig. 3: (a) The persistence function at the putative A_2 transition points, $T = T_d(c)$. The filled symbols are results of the numerical simulation where the system size is $N = 2^{19}$ and the average is taken over 10^2 independent samples. The solid lines are results of power law fitting. (b) The c dependence of the critical exponent a. The filled cycles are data obtained by the numerical simulation. The solid line is the power law fitting which goes to zero at $c = 0.2$.

time increases and $\phi(t)$ develops a plateau. This two-step relaxation behavior is commonly observed for many glassy materials including KCMs on the Bethe lattice *without* random pinning ($c = 0$) [13,34,35]. In the long time limit, $\phi(t)$ converges to a constant value, $\phi(\infty)$, which coincides with ϕ as shown in Fig. 2. The discontinuous jump of ϕ at the transition is directly connected to the two-step relaxation of $\phi(t)$.

At the transition temperature, $T = T_d(c)$, the relaxation of $\phi(t)$ toward $\phi(\infty)$ is well fitted by a power law as expected from MCT;

$$\frac{\phi(t) - \phi(\infty)}{1 - \phi(\infty)} = Bt^{-a}. \tag{1}$$

In Fig. 3 (a), we show the results obtained by fitting the results of our numerical simulations for several c's, where the filled symbols denote the numerical results and the solid lines denote the fits by eq. (1). The values of a for various c's estimated by the numerical simulations are plotted in Fig. 3 (b). The exponent a decreases sharply as c approaches the terminal point of the critical line, *i.e.*, the putative A_3 transition, at $c_c = 0.2$. A qualitatively similar result was obtained for the multi-component extension of the FA model which also exhibits the A_3 transition [34].

The sharp decrease of a is consistent with the result of MCT which predicts that a decreases and eventually vanishes on the A_3 transition point [30]. The vanishing behavior of the critical exponent suggests that eq. (1) should be replaced by a different scaling function at the A_3 transition point. MCT predicts that $\phi(t)$ near the A_3 transition point follows the scaling law [30]:

$$\frac{\phi(t) - \phi_c}{1 - \phi_c} = (T - T_c)^{1/3} f\left((T - T_c)^{1/6} \log(t)\right), \tag{2}$$

where ϕ_c denotes ϕ at the A_3 transition point, (c_c, T_c). The scaling function $f(x)$ behaves as x^{-2} at small argument and linearly (as $ax + b$) at large argument. In order to test this scaling law, we focus on the large x regime[1] in which one should find

$$\frac{\phi(t) - \phi_c}{1 - \phi_c} = -B \log(t/\tau_\beta) \tag{3}$$

with the prefactor B and the relaxation time[2] τ_β scaling as

$$B \propto (T - T_c)^{1/2}, \quad \log \tau_\beta \propto (T - T_c)^{-1/6}. \tag{4}$$

In order to confirm eq. (3), we fix $c = c_c = 0.2$ and calculate $\phi(t)$ for several temperatures slightly above the A_3 transition temperature, $T_c \approx 0.621$. The results are shown in Fig. 4. Near the A_3 transition point, $\phi(t)$ shows single decay instead of the two-step relaxation as shown in Fig. 4. This is consistent with the continuous change of ϕ at the A_3 transition point, as reported in our previous work [26]. In the intermediate time scale where $\phi(t)$ is very close to ϕ_c and the scaling variable x is large, $\phi(t)$ is well fitted by the MCT scaling law, eq. (3), as shown in Fig. 4. B and τ_β obtained by the fitting are shown in Fig. 5 with the scaling law, eq. (4), predicted by MCT. One can see that near the A_3 transition temperature, B and τ_β indeed follow the MCT scaling law. Our results clearly support that the critical dynamic scaling at the terminal point of the random pinning transition line for the FA model is the one predicted by MCT at the A_3 dynamical transition.

Critical Fluctuations. – We now focus on the behavior of dynamic fluctuations that we expect to also become critical at the transition. In particular, we analyze

$$\chi(t) \equiv N\left[\left\langle \phi(t)^2 \right\rangle - \left\langle \phi(t) \right\rangle^2\right], \tag{5}$$

[1] In order to test the small x regime, one would need times much larger than the ones available in our simulations.

[2] We denote the relaxation time τ_β for there are not two distinct regimes at the A_3 critical point but just one, that we denote β.

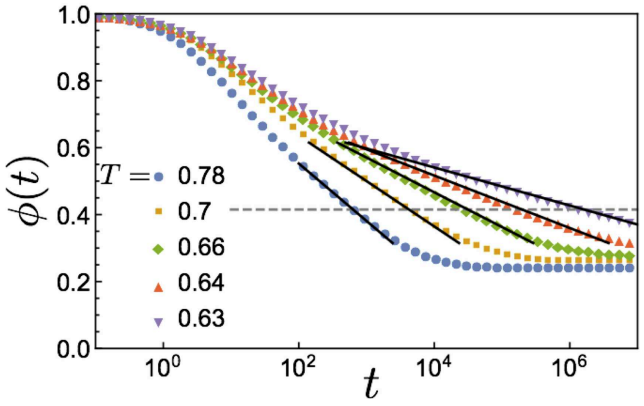

Fig. 4: The persistence functions near the terminal point of the random pinning transition line. The value of the pinned density is fixed at $c = c_c = 0.2$. The filled symbols are simulation results where the average is taken over 10^2 independent samples. The solid lines are logarithmic fit. The horizontal dashed line denotes $\phi_d(c_c)$.

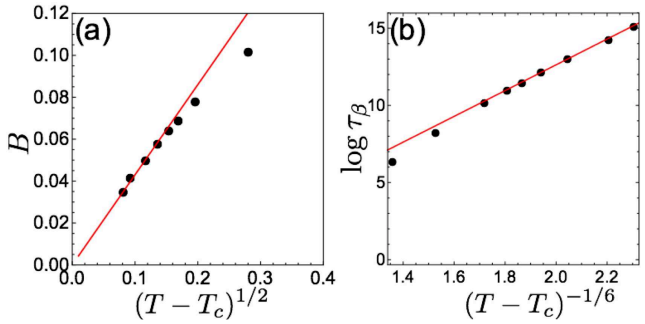

Fig. 5: (a) The temperature dependence of B near the putative A_3 transition temperature T_c. The value of pinned density is fixed at $c = c_c = 0.2$. The filled cycles are results of the numerical simulations where the average is taken over 10^2 independent samples. The solid lines indicate the MCT prediction, $B \propto (T - T_c)^{1/2}$. (b) The temperature dependence of τ_β near the A_3 transition point. The filled symbols represent the numerical results and the solid line represents the MCT prediction, $\log \tau_\beta \propto (T - T_c)^{-1/6}$.

where the bracket denotes the average for both the initial conditions and thermal noises [36]. We calculate $\chi(t)$ approaching a point on the random pinning transition line ($c = 0.05$) and approaching the terminal point ($c_c = 0.2$). The results are shown in Fig. 6 (a) and (b); $\chi(t)$ first increases with t and reaches the maximum, χ^*, at $t = t^*$. At large times $\chi(t)$ decreases and converges to constant values in the long time limit, $\lim_{t\to\infty} \chi(t) = \chi_\infty$. Note that the values of χ_∞ coincide with the fluctuations of the fraction of frozen spins, ϕ, which can be easily calculated by the numerical simulation of the bootstrap percolation (BP). χ_∞ estimated by the BP are shown by solid lines in Fig. 6 (a) and (b).

MCT provides detailed predictions regarding dynamical fluctuation [16,37–39]. In the A_2 case, $\chi(t)$ varies on a time-scale of the order of the relaxation time, displays a diverging peak $\chi^* \propto (T - T_d)^{-2}$, and a featureless long-time limit χ_∞. This is indeed what we find in our numerical simulations, see Fig. 6 (a) and Fig. 7 (a), in agreement with recent results for $c = 0$ [40].

The MCT predictions for the A_3 case are qualitatively different [31][3]:

$$\chi(t) = |T - T_c|^{-4/3}\, g\left((T - T_c)^{1/6} \log(t)\right), \qquad (6)$$

where the scaling function $g(x)$ tends to a constant at large argument hence implying that both χ^* and χ_∞ diverge as $|T - T_c|^{-4/3}$. Again, this is what we find in our numerical simulations, see Fig. 6 (b) and Fig. 7 (b) where we fit the numerical data, as shown by the solid lines in Fig. 7 (b). The agreement is very good, signalling that MCT predictions [31] hold also for the critical behavior of the dynamical fluctuations at the terminal point of the random pinning transition line.

[3]In [31] the IMCT susceptibility was studied, $\chi(t)$ scales as its square as explained in [16, 39].

Self-induced Disorder and Avalanches. – We now show that the criticality found at the terminal point in the FA model is related to self-induced disorder and to the continuous transition along the hysteresis line of the Random Field Ising Model (RFIM) and its avalanches. This is indeed expected since this relationship was shown recently to hold for MCT at the A_3 transitions [16,27,31,41]. Since the critical behavior is presented in both χ^* and χ_∞, we focus on the latter which can be analyzed using BP techniques [13, 42]. The fluctuation of ϕ, which leads to χ_∞, is due to different initial conditions which play the role of the different realization of the quenched randomness [16]. For instance, the initial fraction of the upward spins, p, fluctuates for different initial conditions. This causes sample-to-sample fluctuation, $\delta\phi \propto (\partial\phi/\partial p)\delta p$, and leads to a contribution to the susceptibility which leads $\chi_\infty \propto (\partial\phi/\partial p)^2 \langle \delta p^2 \rangle \propto (\partial\phi/\partial p)^2$. Near the transition point, p can be expressed as a linear function of $T - T_c$ and the derivative by p can be replaced by T. Thus, we obtain $\chi_\infty \propto (\partial\phi(T_c)/\partial T)^2 \propto |T - T_c|^{-4/3}$, which shows the same divergence found for the RFIM at the continuous transition along the hysteresis line. This is not a coincidence; actually all the critical mean-field behavior of the A_3 dynamical transitions, and hence of the terminal point, is the same (see [31] for a detailed comparison) [4]. The previous arguments show that the dynamical critical behavior is produced by the combination of self-induced disorder and the singular dependence of $\phi \sim |T - T_c|^{1/3}$. Let us now unveil that the physical mechanism behind this singular dependence are avalanches identical to the ones

[4]Actually in [31] the comparison was done with the equilibrium continuous RFIM transition which has at the mean-field level the same critical behavior. Following [41] we think that the continuous transition along the hysteresis line is a better comparison from the phenomenological point of view in particular because avalanches appear explicitely.

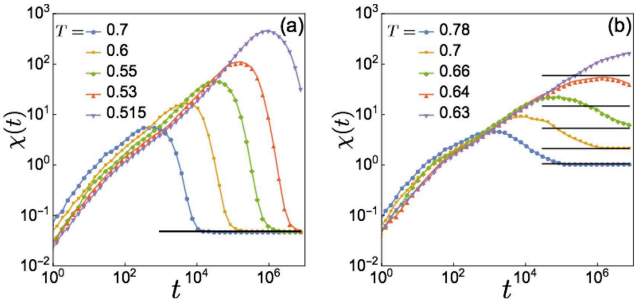

Fig. 6: (a) Susceptibilities near the putative A_2 transition point. The pinned density is fixed at $c = 0.05$. The filled symbols denote the numerical results where the average is taken over 10^2 independent samples. The solid lines denote the values estimated by the bootstrap percolation process (see text). (b) The same date near the putative A_3 transition point. The pinned density is fixed at $c = c_c = 0.2$.

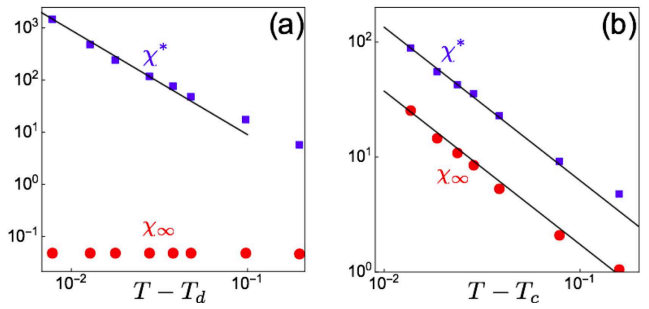

Fig. 7: (a) The peak value of the susceptibilities, χ^*, and the values of the susceptibilities in the long time limit, χ_∞ near the putative A_2 transition temperature. The pinned density is fixed at $c = 0.05$. The filled symbols are results obtained by the numerical simulation. The solid line represent the power law scaling, $\chi^* \propto (T - T_d)^{-2}$. (b) The same date near the putative A_3 transition temperature. The pinned density is fixed at $c = c_c = 0.2$. The filled symbols represent the results obtained by the numerical simulations. The solid line represent the power law scaling, $\chi^* \propto \chi_\infty \propto (T - T_c)^{-4/3}$.

present at the continuous transition along the hysteresis line of the RFIM. The key idea is that by changing the temperature, one changes the fraction of, say, up spins but this in turn leads to a much larger change of blocked spin. The reason is precisely avalanches: by increasing of a factor of two the distance ($\varepsilon = |T - T_c|$) from the transition, a fraction of the order of ε of spins becomes suddenly unblocked because their number of pointing down nearest neighbours becomes larger than $f = 2$. This however leads to a cascade process since some neighbours of the unblocked spins become unblocked and so on and so forth. Thus by changing ε by a factor of two, ϕ decreases by roughly $\varepsilon\langle S\rangle$ where S is the size of the avalanche, *i.e.*, the cascade process discussed above created by unblocking a random spin. By generalizing the computation performed for BP [43] to the $c > 0$ case, we have obtained the distribution function of the size of the avalanche which acquires a scaling form close to the transition at the terminal point [44]:

$$P(S) = \frac{1}{S^\tau} h\left(S|T - T_c|^{4/3}\right), \qquad (7)$$

where $\tau = 3/2$ and the scaling function $h(x)$ coincides with the one computed for the RFIM at the continuous transition along the hysteresis line [45] thus strengthening the relationship discussed above [5]. Using this result, one finds that the average avalanche size scales as $\varepsilon^{-2/3}$ thus leading to $\phi \sim \varepsilon^{1/3}$ and providing the final missing piece to explain the critical behavior at the terminal point. In conclusion, although the explicit time-dependence cannot be obtained in this way, the critical behavior is fully understood even quantitatively in terms of self-induced disorder and avalanches.

Summary and discussion. – We investigated the equilibrium dynamics of the Fredrickson-Andersen model on the Bethe lattice with random pinning as a mean-field model of the dynamical facilitation scenario. We found a dynamical phase diagram qualitatively identical to the one predicted for RFOT (it would be interesting to check whether also the predictions for the aging dynamics hold) [28]. We showed that the persistence function, $\phi(t)$, and the dynamical fluctuations, $\chi(t)$, display a critical behavior consistent with the prediction of the mode coupling theory (MCT) for both the A_2 and A_3 transitions. We also showed that the critical behavior at the terminal point is tightly related to the one of the RFIM and explicitly explained the origin of this relationship in terms of self-induced disorder and avalanches.

Our work fully exposes the universal character of MCT as a generic mean-field dynamical transition. It appears not only in models characterized by rugged energy landscapes but also in models with trivial thermodynamics but glassy dynamics. The predictive power in terms of scaling laws at A_2 and A_3 singularity for the FA model is a remarkable sign that MCT indeed holds also for cooperative KCMs at the mean-field level. In finite dimensions however, fluctuations on top of the mean-field theory are expected to lead to drastic changes [41,47]. Actually, in this case, very different physical mechanisms are expected to be at play for KCMs and systems characterized by rugged energy landscapes respectively. More work is needed—and certainly worth doing— to understand the role of fluctuations and their effect on the mean-field theory.

The other important result of our work is to show explicitly the role of avalanches in determining the MCT critical behavior in agreement with recent results [41]. Although the analysis of avalanches does not allow to determine also time-dependent quantities, the distribution functions of the mobile region for deep supercooled liquids do show similar power law like behaviors [48–50] and

[5] We repeated the computation for transitions in the A_2 universality class and found as expected an avalanche distribution that coincides with the one obtained for the spinodal of the RFIM [46].

sign of avalanche motion in glassy dynamics was found in experiments [51] and in simulations [52]. This is certainly a topic worth further studies both for its theoretical and phenomenological relevance.

* * *

We thank C. Cammarota for feedback and comments on this work. H. I. and K. M acknowledge JSPS KAKENHI Grant Number JP16H04034, JP25103005, JP25000002, and the JSPS Core-to-Core program. H. I. was supported by Program for Leading Graduate Schools "Integrative Graduate Education and Research in Green Natural Sciences", MEXT, Japan and JSPS Grant Number JP16J00389. G. B. acknowledges support from the ERC grants NPRGGLASS and by a grant from the Simons Foundation (#454935, Giulio Biroli)

Appendix. – Here we derive the avalanche distribution of the BP with random pinning on the $z = k + 1$ regular random graph, by generalizing the calculation of the *non*-pinned system [43]. The BP process with random pinning is defined as follows: (1) Prepare the N sites each of which is occupied with probability p. (2) Pick up a faction c of sites randomly and "pin" them. (3) Recursively cull $non - pinned$ sites that have less than m occupied sites in neighbor. Below, we focus on the case when $k = 3$ and $m = 3$ since it corresponds to the model investigated in the main text, see Ref. [13] for more details about the connection between the FA model and BP.

Scaling function of the probability of the occupied sites. First we derive the scaling function for P which is the fraction of the occupied sites after the BP process. To this end, it is more convenient to consider the probability P_* that a occupied site is not culled in the BP process, given that one of the nearest neighbors was occupied. P_* follows the same scaling low of that of P, but is easier to calculate [13]. P_* satisfies the following self-consistent equation [26]:

$$P_* = pc + p(1-c)\left[3P_*^2 - 2P_*^3\right]. \tag{8}$$

It is convenient to introduce the auxiliary function defined by

$$Q(p, c, P_*) = cp + (1-c)p\left[3P_*^2 - 2P_*^3\right] - P_*. \tag{9}$$

At the A_3 transition point, Q should satisfy following equations [35]:

$$\begin{aligned} Q &= cp + (1-c)p\left[3P_*^2 - 2P_*^3\right] - P_* = 0, \\ \frac{\partial Q}{\partial P_*} &= 6(1-c)p(P_* - P_*^2) - 1 = 0, \\ \frac{\partial^2 Q}{\partial P_*^2} &= 6(1-c)p(1-2P_*) = 0. \end{aligned} \tag{10}$$

Solving the above equations, we obtain $c = 1/5$, $p = 5/6$ and $P_* = 1/2$. Expanding Q around this point, one obtains

$$Q = -\frac{4}{3}\delta P_*^3 + \frac{5}{12}\delta c + \frac{3}{5}\delta p - \frac{5}{4}\delta P_* \delta c + \frac{6}{5}\delta P_* \delta p + \dots \tag{11}$$

where $\delta c = c - 1/5$, $\delta p = p - 5/6$ and $\delta P_* = P_* - 1/2$. We decompose vector $(\delta c, \delta p)$ as

$$(\delta c, \delta p) = A\varepsilon_\perp \vec{e}_\perp + B\varepsilon_\parallel \vec{e}_\parallel, \tag{12}$$

where A and B are arbitrary constants. The vectors, $\vec{e}_\perp$ and $\vec{e}_\parallel$, are defined as

$$\vec{e}_\perp = \left(\frac{5}{12}, \frac{3}{5}\right), \qquad \vec{e}_\parallel = \left(-\frac{3}{5}, \frac{5}{12}\right). \tag{13}$$

Substituting eq. (12) into eq. (11), we obtain

$$0 \sim -\frac{4}{3}\delta P_*^3 + \frac{1921}{3600}A\varepsilon_\perp + \frac{5}{4}B\delta P_* \varepsilon_\parallel. \tag{14}$$

Solving above equation, we obtain

$$\delta P * (\varepsilon_\parallel, \varepsilon_\perp) = \left|\varepsilon_\parallel\right|^\beta g\left(\frac{\varepsilon_\perp}{\left|\varepsilon_\parallel\right|^{\delta\beta}}\right), \tag{15}$$

where $\beta = 1/2$ and $\delta = 3$. The scaling function $g(y)$ is the solution of

$$0 = g^3 - \frac{1921}{4800}Ay \mp \frac{15}{16}Bg, \tag{16}$$

where $\pm$ refers to the sign of $\varepsilon_\parallel$. To clarify the connection between this model and the mean-field random-field Ising model, we set $A = \frac{4800}{1921} \times \frac{12\sqrt{2}}{\pi^{3/2}R_c}$ and $B = \frac{16}{15} \times \frac{12}{\pi}$. Then eq. (16) is rewritten as

$$0 = g^3 \mp \frac{12}{\pi}g - \frac{12\sqrt{2}}{\pi^{3/2}R_C}y = 0. \tag{17}$$

Above equation is identical to the scaling function of the order parameter of the mean-field random-field Ising model (see eq. (A.5) in Ref. [46]).

Scaling function of the avalanche distribution. After the BP process, all remained occupied sites which have more than m neighbors of occupied sites are "blocked". Now we randomly cull a occupied site. This leads the avalanche since some neighbors of the culled site become unblocked and so on and so forth. Here we consider the distribution function (denoted as π_a) of the size of the avalanche in a sub-tree connected to the culled site (see Ref. [43] for more precise definition). To this end, it is convenient to introduce the generating function [43]:

$$\pi(x) = \sum_{a=0}^{\infty} \pi_a x^a. \tag{18}$$

$\pi(x)$ satisfies the self-consistent equation:

$$\pi(x) = (1-c)xp\sum_{k=0}^{z-1}\binom{z-1}{k}[\pi(x)]^k\left[1 - P_*\right]^{z-1-k}\delta_{k+1,m} + \pi_0, \tag{19}$$

where

$$\pi_0 = cp + (1-c)p\sum_{k=0}^{z-1}\binom{z-1}{k}[P_*]^k\,[1-P_*]^{z-1-k}\,p_k \tag{20}$$

is the probability that the avalanche does not occur. For $z = 4$ and $m = 3$, the equation is

$$\pi(x) = cp + (1-c)pP_*^3 + 3(1-c)xp(1-P_*)\pi(x)^2. \tag{21}$$

To investigate the avalanche distribution for the large a, we substitute $x = 1-\delta x$ and $\pi(x) = P_* + \delta\pi(x)$ into eq.(21) and obtain

$$\delta\pi^2 + C_1 t\delta\pi - C_2\delta x = 0, \tag{22}$$

where C_1 and C_2 are constants, and we defined

$$t \sim -4\left|\varepsilon_\parallel\right|^{2\beta}\left[g(\varepsilon_\perp/\left|\varepsilon_\parallel\right|^{\delta\beta})^2 \mp \frac{5}{16}B\right]. \tag{23}$$

Solving the above equation, we obtain

$$\delta\pi(x) = \frac{1}{2}\left[-C_1 t + \sqrt{C_1^2 t^2 + 4C_2\delta x}\right]. \tag{24}$$

The asymptotic expression of the π_a for large a is given by

$$\pi_a = \frac{1}{a!}\left.\frac{d^a\pi(x)}{dx^a}\right|_{x=0} \sim \frac{1}{a^{3/2}}e^{-C_3 t^2 a}, \tag{25}$$

where $C_3 = C_1^2/4C_2$. Substituting eq.(23) into eq. (25), one obtains

$$\pi_a(\varepsilon_\parallel,\varepsilon_\perp) \sim a^{-3/2}e^{-16C_3 a\left|\varepsilon_\parallel\right|^{4\beta}\left(g(\varepsilon_\perp/\varepsilon_\parallel^{\delta\beta})^2 \mp \frac{5}{16}B\right)^2}, \tag{26}$$

where $\tau = 3/2$ and $\sigma = 1/4\beta = 1/2$. To see the connection with the RFIM, we set $B = \frac{16}{15}\times\frac{12}{\pi}$, and obtain

$$\pi_a(\varepsilon_\perp,\varepsilon_\parallel) \sim a^{-3/2}e^{-\frac{2^8}{\pi^2}C_3 a\left|\varepsilon_\parallel\right|^{4\beta}\left(1\mp\frac{\pi}{4}g(\varepsilon_\perp/\varepsilon_\parallel^{\delta\beta})^2\right)}. \tag{27}$$

Further, introducing the rescaled avalance size S by

$$a = \frac{\pi^2}{C_3 2^9}S, \tag{28}$$

we obtain

$$\pi_S(\varepsilon_\perp,\varepsilon_\parallel) = S^{-\tau}\mathcal{D}(S/\left|\varepsilon_\parallel\right|^{-1/\sigma}, \varepsilon_\perp/\left|\varepsilon_\parallel\right|^{\beta\delta}), \tag{29}$$

with the critical exponents $\tau = 3/2$, $\sigma = 1/2$, $\beta\delta = 3/2$, and the scaling function

$$\mathcal{D}(x,y) = e^{-x\left[1\mp\frac{\pi}{4}g(y)^2\right]^2/2}. \tag{30}$$

This equation corresponds to the scaling function of the avalanche distribution of the random field Ising model (see eq. (A12) in Ref. [46]). To derive eq. (12) in the main text, one should note that $\varepsilon_\perp \sim \left|\varepsilon_\parallel\right| \sim |T-T_c|$ and $\varepsilon_\perp/\left|\varepsilon_\parallel\right|^{\beta\delta} \gg 1$ for general directions. Using $g(y) \sim y^{1/3}$ ($y \gg 1$), one arrives at the asymptotic form of the avalanche distribution function

$$P(S) \sim \pi_S \sim S^{-\tau}e^{-CS|T-T_c|^{4/3}}, \tag{31}$$

where C is a constan.

REFERENCES

[1] Debenedetti P. G. and Stillinger F. H., *Nature*, **410** (2001) 259.
[2] Berthier L. and Biroli G., *Rev. Mod. Phys.*, **83** (2011) 587.
[3] Biroli G. and Garrahan J. P., *J. Chem. Phys.*, **138** (2013) 12A301.
[4] Bengtzelius U., Gotze W. and Sjolander A., *J. Phys. C*, **17** (1984) 5915.
[5] Götze W., *Complex Dynamics of Glass-Forming Liquids: A Mode-Coupling Theory* Vol. 143 (OUP Oxford) 2008.
[6] Brambilla G., El Masri D., Pierno M., Berthier L., Cipelletti L., Petekidis G. and Schofield A. B., *Phys. Rev. Lett.*, **102** (2009) 085703.
[7] Kirkpatrick T. R. and Wolynes P. G., *Phys. Rev. A*, **35** (1987) 3072.
[8] Kirkpatrick T., Thirumalai D. and Wolynes P. G., *Phys. Rev. A*, **40** (1989) 1045.
[9] Bouchaud J.-P. and Biroli G., *J. Chem. Phys.*, **121** (2004) 7347.
[10] Chandler D. and Garrahan J. P., *Annu. Rev. Phys. Chem.*, **61** (2010) 191.
[11] Ritort F. and Sollich P., *Adv. Phys.*, **52** (2003) 219.
[12] Fredrickson G. and Andersen H., *Phys. Rev. Lett.*, **53** (1984) 1244.
[13] Sellitto M., Biroli G. and Toninelli C., *EPL*, **69** (2005) 496.
[14] Sellitto M., *Phys. Rev. Lett.*, **115** (2015) 225701.
[15] Andreanov A., Biroli G. and Bouchaud J.-P., *EPL*, **88** (2009) 16001.
[16] Franz S., Parisi G., Ricci-Tersenghi F. and Rizzo T., *Eur. Phys. J. E Soft Matter*, **34** (2011) 1.
[17] Franz S., Parisi G. and Ricci-Tersenghi F., *J. Stat. Mech. Theor. Exp.*, **2013** (2013) L02001.
[18] Franz S. and Sellitto M., *J. Stat. Mech. Theor. Exp.*, **2013** (2013) P02025.
[19] Kim K., *EPL*, **61** (2003) 790.
[20] Krakoviack V., *Phys. Rev. Lett.*, **94** (2005) 065703.
[21] Karmakar S., Lerner E. and Procaccia I., *Physica A: Statistical Mechanics and its Applications*, **391** (2012) 1001.
[22] Jack R. L. and Berthier L., *Phys. Rev. E*, **85** (2012) 021120.
[23] Cammarota C. and Biroli G., *PNAS*, **109** (2012) 8850.
[24] Kob W. and Berthier L., *Phys. Rev. Lett.*, **110** (2013) 245702.
[25] Ozawa M., Kob W., Ikeda A. and Miyazaki K., *PNAS*, **112** (2015) 6914.
[26] Ikeda H. and Miyazaki K., *EPL*, **112** (2015) 16001.
[27] Cammarota C. and Biroli G., *J. Chem. Phys.*, **138** (2013) 12A547.
[28] Cammarota C. and Biroli G., *EPL*, **98** (2012) 16011.
[29] Szamel G. and Flenner E., *EPL*, **101** (2013) 66005.
[30] Gotze W. and Sjogren L., *J. Phys. Condens. Matter*, **1** (1989) 4203.
[31] Nandi S. K., Biroli G., Bouchaud J.-P., Miyazaki K. and Reichman D. R., *Phys. Rev. Lett.*, **113** (2014) 245701.
[32] Chalupa J., Leath P. L. and Reich G. R., *J. Phys. C*, **12** (1979) L31.
[33] Krauth W., *Algorithms and computations* (2006).

[34] Arenzon J. J. and Sellitto M., *J. Chem. Phys.*, **137** (2012) 084501.
[35] Sellitto M., *J. Chem. Phys.*, **138** (2013) 224507.
[36] Berthier L., Biroli G., Bouchaud J.-P. and Jack R. L., *Dynamical Heterogeneities in Glasses, Colloids, and Granular Media* (Oxford University Press New York, Oxford) 2011 Ch. 3 p. 68.
[37] Franz S. and Parisi G., *J. Phys. Condens. Matter*, **12** (2000) 6335.
[38] Biroli G., Bouchaud J.-P., Miyazaki K. and Reichman D. R., *Phys. Rev. Lett.*, **97** (2006) 195701.
[39] Berthier L., Biroli G., Bouchaud J.-P., Kob W., Miyazaki K. and Reichman D. R., *J. Chem. Phys.*, **126** (2007) 184504.
[40] de Candia A., Fierro A. and Coniglio A., *Sci. Rep.*, **6** (2016) .
[41] Nandi S. K., Biroli G. and Tarjus G., *Phys. Rev. Lett.*, **116** (2016) 145701.
[42] Branco N., *J. Stat. Phys.*, **70** (1993) 1035.
[43] Shukla P., *Pramana*, **71** (2008) 319.
[44] See supplemental material at [URL inserted by EPL].
[45] Sethna J. P., Dahmen K., Kartha S., Krumhansl J. A., Roberts B. W. and Shore J. D., *Phys. Rev. Lett.*, **70** (1993) 3347.
[46] Dahmen K. and Sethna J. P., *Phys. Rev. B*, **53** (1996) 14872.
[47] Rizzo T., *EPL*, **106** (2014) 56003.
[48] Donati C., Glotzer S. C., Poole P. H., Kob W. and Plimpton S. J., *Phys. Rev. E*, **60** (1999) 3107.
[49] Weeks E. R., Crocker J. C., Levitt A. C., Schofield A. and Weitz D. A., *Science*, **287** (2000) 627.
[50] Gebremichael Y., Vogel M. and Glotzer S., *J. Chem. Phys.*, **120** (2004) 4415.
[51] Candelier R., Dauchot O. and Biroli G., *Phys. Rev. Lett.*, **102** (2009) 088001.
[52] Candelier R., Widmer-Cooper A., Kummerfeld J. K., Dauchot O., Biroli G., Harrowell P. and Reichman D. R., *Phys. Rev. Lett.*, **105** (2010) 135702.